JOURNAL OF GEOPHYSICAL RESEARCH, VOL. 99, NO. D10, PAGES 20,623–20,631, OCTOBER 20, 1994

Vertical structure of atmospheric gravity waves revealed by the wavelet analysis

Kaoru Sato
Center for Climate System Research, University of Tokyo

Michio Yamada
Department of Mathematical Sciences, University of Tokyo

Abstract. It is well known that the vertical wavenumber (m) spectra of temperature and horizontal wind fluctuations have a steep slope (almost proportional to m^{-3}) in the middle atmosphere. These spectra are considered to be due to saturated gravity waves. However, since power spectral analysis assumes sinusoidal waves with constant amplitudes in the height region for which the spectra are calculated, the information on the height position, where the disturbance having each wavenumber is dominant, is lost. In this paper the dominant height position is examined using a recently developed wavelet method. An analysis is made of temperature observation data by radiosondes and wind data by a mesosphere, stratosphere, and troposphere (MST) radar in the lower stratosphere. It is shown that the height where the variance is largest increases with the wavenumber. This variation with wavenumber is explained well by a monochromatic inertia-gravity wave whose vertical wavenumber changes due to the vertical shear of the large-scale background wind during its vertical propagation. Thus we consider theoretically the vertical wavenumber spectrum of a single saturated gravity wave which propagates upward in a large-scale background wind with a vertical shear. The slope of the theoretical spectrum is steep (proportional to m^{-4} or m^{-3} depending on m for a linear shear) and similar to the observations. The result suggests that the vertical shear of large-scale wind structure plays an important role in determining the shape of universal m spectra in the middle atmosphere.

1. Introduction

Recent progress of the mesosphere, stratosphere, and troposphere (MST) radars, Rayleigh and Na lidars, and radiosondes enables us to examine the wind and temperature fluctuations in the middle atmosphere in terms of the spectra. In particular, it has been known that power spectra versus vertical wavenumber (m) of horizontal wind and temperature fluctuations commonly have a shape with a steep slope of about m^{-3} in a higher wavenumber region [e.g., *Gardner and Voelz*, 1987; *Tsuda et al.*, 1989; *Wilson et al.*, 1991]. The characteristic wavenumber m_*, that is, the lowest wavenumber of the m^{-3} region, corresponds to a vertical wavelength λ_z ($\equiv 2\pi/m$) of 2–3 km in the lower stratosphere. The m^{-3} spectra have been attributed by several theoretical studies to so-called saturated gravity waves whose amplitudes are limited by wave breaking due to a local convective instability [e.g., *Dewan and Good*, 1986], or by wave-wave interactions through the diffusion process [*Weinstock*, 1990] and/or through the advection process, namely, the Doppler spreading effect [*Hines*, 1991b].

It is considered that local convective instability limits the horizontal wind amplitude of a saturated gravity wave to N/m [e.g., *Fritts*, 1984]. Assuming the spectral region occupied by one saturated gravity wave, Δm, is proportional to the wavenumber m, *Dewan and Good* [1986] argued that the spectrum should be proportional to N^2/m^3. The validity of the assumption, however, has not been confirmed and the argument itself has been challenged [*Hines*, 1991a]. *Smith et al.* [1987] further examined the effect of superposition of gravity waves obeying a universal gravity wave spectral model by *VanZandt* [1985] and obtained the spectral amplitude of $1/6\ N^2/m^3$ for $m \gtrsim m_*$. They used a saturation in which the variance of temperature fluctuations due to gravity waves is suppressed so as not to make the total lapse rate superadiabatic. Their spectra have been widely accepted because the amplitude accords well with many observations. It should be noted, however, that VanZandt's model determines the spectral shape, namely, m^{-3} for m spectra, a priori from the observations and does not predict it theoretically.

Fourier spectrum analysis assumes a constant amplitude for each sinusoidal wave having a given wavelength (or frequency) over the whole data series and therefore does not provide information on the positions where each disturbance is dominant in the data series. Although a lot of efforts have been devoted to the m spectrum of temperature and horizontal wind fluctuations, there are only a few studies on the vertical energy distribution of fluctuations having each m. Recently, *Sato* [1994, hereinafter referred to as S94] examined statistically the structure of inertia-gravity waves which are dominant in the lower stratosphere. The wave parameters were estimated as a function of height by fitting wind fluctuations in each small height region to a sinusoidal wave under the assumption of local monochromaticity. Such stud-

Paper number 94JD01818.
0148-0227/94/94JD-01818$05.00

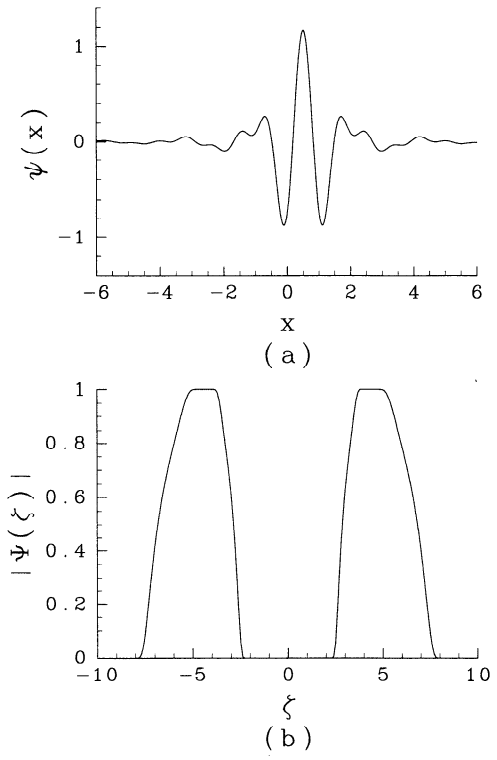

Figure 1. (a) Meyer's wavelet $\psi(x)$. This is a smooth (infinitely differentiable) function which is symmetric and localized around $x = 1/2$. (b) Fourier transform of Meyer's mother wavelet. Only the modulus of the Fourier transform, $|\hat{\psi}(\zeta)|$, is shown in this figure. The Fourier transform is not zero only for $-8\pi/3 < \zeta < -2\pi/3$ and $2\pi/3 < \zeta < 8\pi/3$.

ies are important to elucidate the physical processes which produce the observed spectra having the characteristic shape.

The wavelet method adopted in this study provides information on the vertical variation of an m spectrum and is applied to temperature fluctuations in the lower stratosphere observed by radiosondes. To interpret the vertical structure of fluctuations revealed by the wavelet analysis, we consider the effect of the vertical shear of the large-scale background wind on the change of vertical wavelength of a single gravity wave propagating vertically. Moreover, a theoretical m spectrum due to such a single gravity wave is obtained under the WKB approximation, and compared with observations.

2. Wavelet Analysis

Fourier transform method is a fundamental tool for data analyses in meteorology. A given data series is Fourier decomposed into several components of different length scales, and this decomposition gives us an insight into physical mechanisms underlying the data series. However, when a data series includes different kinds of events, the Fourier spectrum is usually a complex mixture which is difficult to interpret even if each event has a clear and simple form of Fourier spectrum. One of the reasons for this difficulty is that the Fourier spectrum, the squared modulus of the Fourier coefficients, lacks the information of the position of the events, which is carried in the phases of the Fourier coefficients.

The orthonormal wavelet expansion, which we are going to employ in our analysis, allows us a position-wavenumber analysis, in which we can identify positions of the events corresponding to wavenumber structures observed in the Fourier spectrum. The orthonormal wavelet analysis is a novel tool of data analysis, which was first invented in the 1980s by *Stromberg* [1982] and *Meyer* [1985] independently and has been a subject of intense investigation [see *Daubechies*, 1988, 1992]. In the present paper we are interested in the positions of the events responsible for wavenumber components of temperature profiles observed by radiosondes, and we employ an orthonormal wavelet of the Meyer type in our analysis. Below we describe only practical features of the orthonormal wavelet without going into its mathematical details. Readers who are interested in detailed aspects of the orthonormal wavelet should consult with references [*Meyer*, 1985; *Daubechies*, 1992; *Yamada and Ohkitani*, 1990, 1991a, b].

The basic idea of orthonormal wavelet analysis is to expand a given data by basis functions more localized than sinusoidal functions. These basis functions called orthonormal wavelets (or simply wavelets) are constructed from an appropriately localized function $\psi(x)$ called the analyzing or mother wavelet as follows:

$$\psi_{j,k}(x) = 2^{j/2}\psi\left(2^j\left(x - \frac{k}{2^j}\right)\right), \qquad j,\ k \text{ are integers}, \tag{1}$$

which is the mother wavelet dilated by 2^j and translated by $k/2^j$. The prefactor $2^{j/2}$ is inserted only to make its norm, $\int_{-\infty}^{\infty} |\psi_{j,k}(x)|^2\, dx$, unity. Note that $\psi_{j,k}$ is more localized in real space for larger j. Here we chose a special type of mother wavelet, as shown in Figure 1a [*Meyer*, 1985; *Yamada and Ohkitani*, 1990], so that $\psi_{j,k}$ can form a complete orthonormal basis. As seen in Figure 1a, this mother wavelet is a smooth function (i.e., infinitely differentiable) which is well localized in real space around its symmetric axis at $x = 1/2$. In wavenumber space, on the other hand, this mother wavelet has a compact support, i.e., Fourier transform of $\psi(x)$ is zero except for $x \in [-8\pi/3, -2\pi/3] \cup [2\pi/3, 8\pi/3]$ (Figure 1b). Therefore $\psi(x)$ is well localized both in real and in wavenumber spaces.

The mother function is constructed very carefully in order that the wavelets $\psi_{j,k}$ constitute an orthonormal basis. Below we only summarize a construction method of this mother wavelet without proof.

$$\psi(x) = \frac{1}{2\pi}\int_{-\infty}^{\infty} \exp\,[ikx]\hat{\psi}(k)\ \mathrm{d}k, \tag{2}$$

$$\hat{\psi}(k) = \exp\left[-\frac{ik}{2}\right]\sqrt{\phi\left(\frac{k}{2}\right)^2 - \phi(k)^2}, \tag{3}$$

$$\hat{\phi}(k) = \sqrt{g(k)g(-k)}, \tag{4}$$

$$g(k) = \frac{h\left(\frac{4\pi}{3} - k\right)}{h\left(k - \frac{2\pi}{3}\right) + h\left(\frac{4\pi}{3} - k\right)}, \tag{5}$$

$$h(k) = \begin{cases} \exp\,[-1/k^2] & (k > 0), \\ 0 & (k \le 0). \end{cases} \tag{6}$$

We now introduce the orthonormal wavelet expansion. Suppose that the data $f(x)$ is expanded by orthonormal wavelets as follows:

$$f(x) = \sum_{j=-\infty}^{\infty} \sum_{k=-\infty}^{\infty} \alpha_{j,k}\psi_{j,k}(x) \tag{7}$$

where $\alpha_{j,k}$ are expansion coefficients. Remembering that $\psi_{j,k}$ is the dilated and translated mother wavelet $\psi(x)$ which is well localized in real and wavenumber spaces, we see that the above expansion is a decomposition of the data into components of wavenumber $\sim 2^j$ and spatial position $\sim k/2^j$, of which the magnitudes are given by $\alpha_{j,k}$.

The orthonormality together with the well localization of the basis functions $\psi_{j,k}$ allow us to interpret $|\alpha_{j,k}|^2$ as the energy of the component corresponding to wavenumber $\sim 2^j$ located at the position $\sim k/2^j$. For this reason we call $|\alpha_{j,k}|^2$ the wavelet spectrum below. Now if we sum up these squared coefficients over the position parameter k, the result is related to the Fourier spectrum $P(\zeta)$ as follows:

$$\sum_{k=-\infty}^{\infty} |\alpha_{j,k}|^2 \sim \zeta P(\zeta) \tag{8}$$

where the nondimensional wavenumber ζ is roughly equal to $(2^{j+2}/3)\pi$. Here the multiplication of ζ by $P(\zeta)$ is due to the fact that Fourier spectrum of $\psi_{j,k}$ does not vanish over a wavenumber band of which the width is proportional to $2^j(\propto\zeta)$. This relation means that if $P(\zeta)$ is proportional to ζ^{-t}, then $\sum_{k=-\infty}^{\infty} |\alpha_{j,k}|^2$ is proportional to $\zeta^{-(t-1)} \sim 2^{-(t-1)j}$, and vice versa. We also note that the right-hand side is independent of unit we employ; i.e., $\zeta P(\zeta) = mP(m)$, where m is the dimensional vertical wavenumber which is proportional to ζ. For numerical calculation we adopt the fast algorithm devised for Meyer type wavelet by *Yamada and Ohkitani* [1990], which employs fast Fourier transform to reduce central processing unit time. We would like to stress that the interpretation of the squared coefficient $|\alpha_{j,k}|^2$ as energy is possible only in the case of an orthonormal wavelet, while in the case of a continuous wavelet we always have to be careful with unphysical relations arising from overcompleteness of the wavelets.

3. Application of Wavelet Analysis to Observation Data

3.1. Data Description

Analyzed are the temperature data from six radiosondes launched at the site of the middle and upper atmosphere (MU) radar (one of the MST radars; 35°N, 136°E, Shigaraki, Shiga, Japan) every 12 hours on October 18–21, 1988. We also use the line-of-sight wind velocities in the vertical direction and in the east, west, north, and south directions at the same zenith angle of 12° that were obtained every 6 min by a simultaneous observation for 72 hours by the MU radar (see *Fukao et al.* [1985a, b] for the detailed system). It is noted that the MU radar site is 370 m above sea level and that all altitudes described in this paper are above the ground level.

Figure 2a shows the mean vertical profile of temperature (T) together with the standard deviation of fluctuation components. The tropopause is located at an altitude of about 16 km. It should be noted that there is no large difference in the standard deviation between the troposphere and lower stratosphere. Mean zonal (V_E) and meridional (V_N) winds and their standard deviations are also plotted in Figures 2b and 2c, respectively. A peak of the subtropical westerly jet is observed around an altitude of 13 km and the zonal wind becomes almost zero around 20 km.

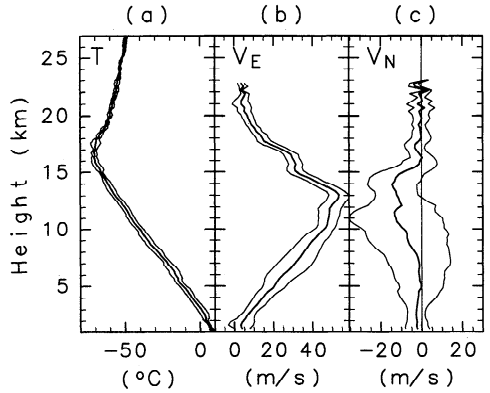

Figure 2. Vertical profiles of the (a) time mean temperature T, (b) zonal wind V_E, and (c) meridional wind V_N together with their standard deviations on October 18–21, 1988.

3.2. Wavelet Spectrum

Wavelet analysis is performed for the temperature data, whose nominal vertical resolution is so fine (about 10 m) compared with the vertical resolution of the MU radar data (about 300 m) that the temperature spectra extend to higher m values. We used six vertical profiles of temperature deviations from the vertical mean for the height region below 27 km in which all of the six radiosonde soundings were successful. Since the algorithm adopted here is available only for data series having 2^n points (n is an integer), we made data series having 4096 ($= 2^{12}$) points in a height region of 0–40.95 km with an interval of 10 m, by adding zero values for the region of 27.01–40.95 km.

First, the mean wavelet spectrum is obtained by averaging the wavelet spectra derived from the six data series. The mean wavelet spectrum is then weighted by 2^j to produce an energy content form of $|\alpha_{j,k}|^2 \times 2^j$ which we hereinafter call variance. Note that this variance has a unit of K^2 and is corresponding to the Fourier spectrum in an energy content form of $mP(m)$. Figure 3 shows a contour map in m-z space of the variance using a logarithmic scale for m, where z is the altitude. The contour intervals were taken to be equal steps in the logarithm of the weighted spectrum. The wavelet position j ($= 3, 4, \cdots, 9$) is corresponding to the wavenumber m of $\sim(2^{j+2}/3)\pi/H$, where H is the height expanse of 4.095×10^4 m for which the wavelet spectrum is calculated. Tick marks on the top axis denote the wavelet positions in m space shown by the bottom axis.

At most heights the logarithm of the spectral amplitude decreases almost monotonically as (the logarithm of) m increases in the region where m is greater than 3×10^{-3} m^{-1}, as denoted by the arrow. This means that the spectra are of a power law type of m^t ($t < 0$) at respective heights. An interesting feature is that the contour lines are not

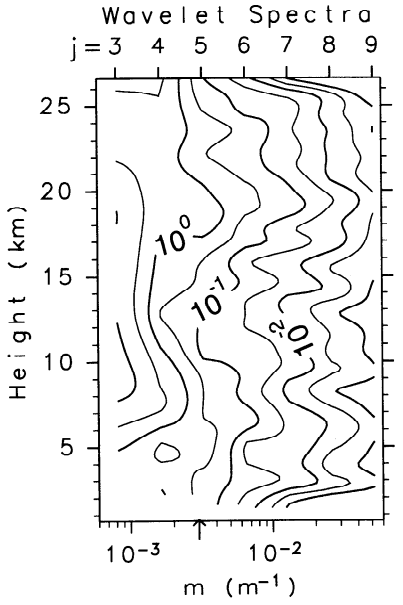

Figure 3. A wavelet spectrum in the energy content form (namely, weighted by m) of the temperature fluctuations averaged for the six profiles on October 18–21, 1988. Numerals on the thick contours show the spectral values in K^2. The thin contours are drawn for 3×10^0, 3×10^{-1}, 3×10^{-2}, $\cdots$ (K^2).

parallel to the height axis even within the stratosphere, indicating that the distribution of the variance at each m is not uniform through the whole height region. In particular, the contour lines are slanted in a region of 16–19 km in the stratosphere (hereafter referred to as region A). In other words, the spectral amplitudes at larger m values increase with height in region A.

We can find the heights where the variance is largest at each m, by normalizing the variances by their vertical mean for each m. The obtained normalized wavelet spectrum is shown in Figure 4. Units of the contours are decibels. It is found that the heights with large variances depend on m. For example, in the troposphere, large variances at m values larger than 7×10^{-3} m^{-1} are observed at heights of 3, 6, and 10 km corresponding to inversion layers, though these layers are hardly recognized in the averaged profile of Figure 2a. The variances at smaller m values are large in a relatively broad height region of 7–11 km. It is remarkable for the lower stratosphere that in region A the height with the largest variance appears to increase with m when m is larger than 3×10^{-3} m^{-1}. The broken line is a theoretical line to be explained in section 4.

The vertical wavelength of a gravity wave changes according to the vertical variation of the large-scale background wind through which the wave propagates. The dispersion relation for an internal gravity wave,

$$\hat{\omega}^2 = \frac{k^2}{m^2} N^2 \qquad (f^2 \ll \hat{\omega}^2 \ll N^2) \tag{9}$$

indicates the vertical wavenumber m changes according to the background wind speed as

$$|m(z)| \sim \frac{N}{|\hat{c}(z)|} \equiv \frac{N}{|c - U(z)|}, \tag{10}$$

under the WKB approximation, where N is the Brunt-Väisälä frequency, $\hat{\omega}$ is the intrinsic frequency for the gravity wave, k is the horizontal wavenumber, $\hat{c}$ ($\equiv \hat{\omega}/k$) is the intrinsic horizontal phase speed, c is the ground-based horizontal phase speed, and $U(z)$ is the background wind speed in the direction parallel to $\hat{c}$. For example, the vertical wavelength of a gravity wave approaching its critical level of z_c, where $U(z_c) = c$, decreases monotonically. For hydrostatic inertia-gravity waves the dispersion relation becomes

$$\hat{\omega}^2 = f^2 + \frac{k^2}{m^2} N^2, \tag{11}$$

and hence the relation between m and U is

$$m(z)^2 = \frac{N^2}{|c - U(z)|^2 - f^2/k^2}, \tag{12}$$

where f is the inertial frequency. Inertia-gravity waves encounter another critical level (the so-called Jones critical level [*Jones*, 1967]) where $|c - U(z)| = |f/k|$, before it reaches the level where $|c - U(z)| = 0$. It is also expected for an inertia-gravity wave that the vertical wavelength decreases monotonically as the wave approaches the Jones critical level. The increase of the height having large variance with m observed in region A may be due to a gravity wave approaching its critical level. The critical level may be at about 20 km in the present case since the large variances are not observed above that height. Thus we examine the

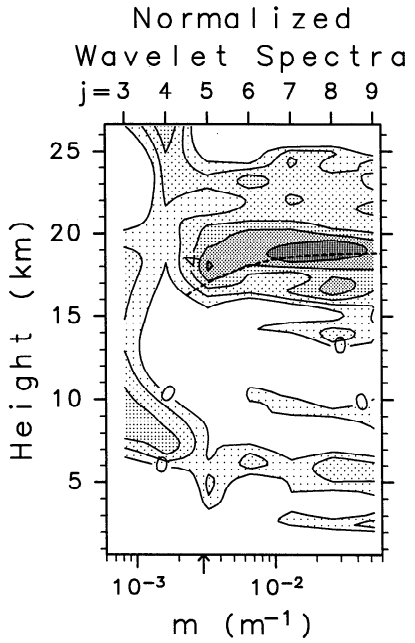

Figure 4. The same as Figure 3 but for the wavelet spectrum normalized by the vertical mean for each m. Units are decibels. Regions with larger spectral amplitudes are shaded with darker patterns. The dotted curve shows a theoretically estimated vertical wavenumber which changes with height due to the vertical variation of the large-scale background wind.

wave structure further from the viewpoint of a single propagating gravity wave.

4. Wave Parameter Estimation

The critical level is estimated from the observation data under the assumption of local monochromaticity. Figure 5 is an example of unfiltered temperature profiles analyzed by the wavelet method. Decrease of the vertical wavelength of temperature fluctuations with height is very clear in region A. This corresponds to the feature in the wavelet spectrum where the height having large variance increases with m. Similar tendency is also observed for the other five profiles, though not so clearly as in Figure 5.

In the lower stratosphere, inertia-gravity waves with short vertical wavelength and long period are dominant and most of them propagate energy upward in all seasons (S94). It is likely that the fluctuation observed in Figure 5 is also due to one such inertia-gravity wave. Thus we estimate the phase velocity under the assumption that it is an inertia-gravity wave.

The horizontal wind fluctuations due to the inertia-gravity wave are extracted using both a low-pass filter with a cutoff length of 10 hours in time and a high-pass filter with a cutoff length of 4 km in height, following S94. The short-period fluctuations are removed to reduce error in the phase velocity estimation, although the fluctuations with periods shorter than 10 hours are negligibly small. The temperature component of the inertia-gravity wave is obtained using a high-pass filter in height with the same cutoff length as that for the horizontal wind components.

The horizontal wind component v', which is counterclockwise perpendicular to the intrinsic phase velocity, is related to the temperature component T' as follows:

$$\frac{T'}{\bar{T}} = -\frac{N^2 k}{mgf} v', \tag{13}$$

where g is the acceleration due to gravity. Therefore for an inertia-gravity wave propagating energy upward (downward), T' is in phase (in antiphase) with v' since m is negative (positive).

The sign of m can be estimated from the hodograph of the horizontal wind component of the inertia-gravity wave.

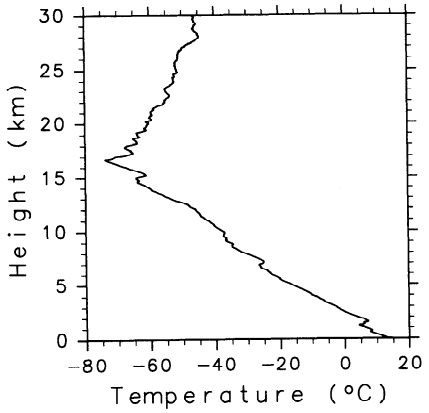

Figure 5. Unfiltered vertical profile of the temperature obtained by a radiosonde on 0800 local standard time (LST) October 19, 1988.

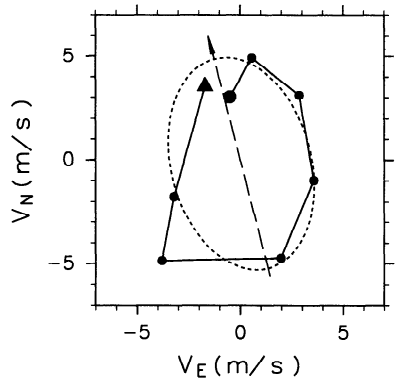

Figure 6. Hodograph of the horizontal wind fluctuations in the 16- to 18-km height region at 0800 LST October 19, 1988. Note that the rightward and upward directions show eastward and northward winds, respectively. Dots show the positions where the data exist. The large circle and triangles denote heights of 16 and 18 km, respectively. The dotted ellipse is the hodograph assumed for the wave parameter estimation. The broken arrow shows the direction of intrinsic phase velocity estimated from the phase difference between temperature and horizontal wind fluctuations.

Figure 6 shows the hodograph of horizontal wind fluctuations in the 16- to 18-km region at the same observation time as that of the temperature data in Figure 5. The hodograph rotates clockwise with height, which indicates that the inertia-gravity wave propagates energy upward, namely, m is negative.

The direction of horizontal intrinsic phase velocity is estimated by examining the phase difference between temperature and horizontal wind components. A large negative maximum is observed at 16.6 km in the temperature profile in Figure 5. Equation (13) indicates that the v' profile should take its negative peak at the same height of 16.6 km. Thus the height position of the negative peak of v' is obtained in the range of 16–18 km by assuming various directions of the intrinsic phase velocity. The height position is determined in the following way. First, we obtain the height h_{max} where v' takes a negative maximum in the discrete data series with the height interval of about 300 m. Then the negative peak position is estimated as the average of five heights having negative v' around h_{max} weighted with the absolute value of v'. The result is shown in Figure 7 as a function of assumed intrinsic phase velocity direction. It is found that the intrinsic phase velocity is in the direction of 14.5° west of north, where the heights of negative peaks of T' and v' accord. Also inertia-gravity wave theory dictates that the long axis of the hodograph ellipse is parallel to the intrinsic phase velocity. The dashed arrow in Figure 6 shows the intrinsic phase velocity direction obtained using (13), which is almost equal to the direction of the long axis. This fact confirms the validity of the assumption of the inertia-gravity wave.

Figure 8 shows the profiles of mean wind, temperature fluctuations (T'), and horizontal wind component parallel to (u') and perpendicular to (v') the intrinsic phase velocity. The phases of T' and v' accord well in a height region of 16–18 km, while the correspondence is unclear above. The tendency of a vertical wavelength decrease with height, clear in the T' profile, is not observed in the v' and u' profiles. These unclear features in u' and v' profiles are probably due

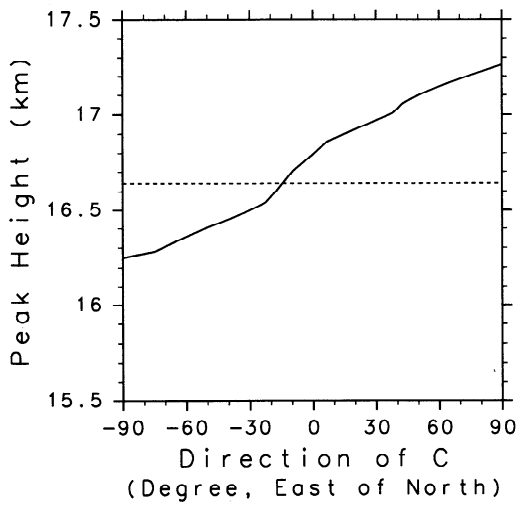

Figure 7. The height where v' takes its negative peak in the range of 16–18 km as a function of assumed direction of the intrinsic phase velocity.

to the aliasing from the low resolution of radar observation. The radar resolution of about 300 m is too low to detect the vertical wavelength if it is shorter than 1 km above the 18-km height, as is clearly observed in the T' profile by radiosondes having a nominal resolution of 10 m. Therefore we estimate the magnitude of phase velocity from the profiles of T', u', and v' in the 16- to 18-km height region. We may note here that a large fluctuation is observed in u' and v' at 19.5–20 km. Judged from the fact that the ratio of amplitude of u' to that of T' is apparently different between the two height regions around 19.5 and 16.5 km, this fluctuation is considered to be due to different inertia-gravity waves from that in the lower region examined in this section.

The shape of a hodograph is affected by the vertical shear of background horizontal wind (V_z) perpendicular to the intrinsic phase velocity [*Hines*, 1989], and the shearing effect is important for the estimation of horizontal wavenumber (S94). In our case, the intrinsic phase velocity is almost northward, and therefore the direction of V_z is eastward. The V_z may not be negligible because of the subtropical westerly jet (see the dashed curve in Figure 8a). In such cases the polarization relation between u' and v' is modified to

$$u' = -\frac{im\hat{\omega}}{V_z k - mf} v', \tag{14}$$

and the dispersion relation becomes

$$\hat{\omega}^2 = f^2 + \frac{N^2 k^2}{m^2} - \frac{f V_z k}{m} \tag{15}$$

(S94). Here it should be noted that (13) is also modified to

$$\frac{T'}{\bar{T}} = -\frac{N^2 k}{g(mf - V_z k)} v'. \tag{16}$$

However, since V_z is positive (and m is negative) in the present case, the phase difference between T' and v' is not changed by the modification.

The hodograph in Figure 6 is approximated to an ellipse denoted by a dotted curve having vertical wavenumber m of 3.3×10^{-3} rad/m^{-1} (about 1.9 km in vertical wavelength) and the amplitudes of u' and v' of 5.2 and 3.4 m s^{-1}, respectively. Using the value of 8×10^{-3} s^{-1} as V_z, 2.1×10^{-2} s^{-1} as N, and 8.3×10^{-5} s^{-1} as f, k, and $\hat{\omega}$ are estimated from (14) and (15) as 3.8×10^{-5} m^{-1} (160 km in horizontal wavelength) and 2.7×10^{-4} rad s^{-1} (6.6 hours in intrinsic period), respectively. Thus the intrinsic phase velocity $\hat{c}$ is estimated as 7.0 m s^{-1}. Since the large-scale background wind U in the direction of $\hat{c}$ is -7.5 m s^{-1}, the ground-based phase speed c is almost zero. Thus Jones critical level for this inertia-gravity wave is located at about 19 km where the background wind speed is equal to f/k ($\approx$2 m s^{-1}), which is consistent with the speculation in the previous section from the wavelet spectrum (Figure 4).

The decrease of vertical wavelength with height can be explained by the effect of the vertical shear of large-scale background wind on a single inertia-gravity wave propagating vertically. Using the obtained ground-based phase velocity ($c \approx 0$ m s^{-1}) we can estimate the vertical wavelength at each height using (15), namely, 2.9 km at 16 km, 2.1 km at 17 km, and 1.1 km at 18 km. These accord well with the vertical wavelengths observed in the temperature fluctuations (Figure 8). It is worth noting that the vertical wavelength estimation using (12) provides almost the same results (the difference is less than 10%), indicating that the effect of V_z is small for the estimation of m, although it is large for the estimation of k and $\hat{\omega}$. The estimated vertical wavelengths are plotted by a dashed curve as a function of height in the wavelet spectra of Figure 4. The dashed curve traces almost exactly the heights where the variance at each m is largest. This agreement supports that the characteristic vertical structure of temperature fluctuations revealed by the wavelet analysis is due to a single gravity wave propagating upward and indicates that the effect of the vertical variation of the large-scale background wind $U(z)$ is important to determine the distribution of the vertical wavelength of gravity waves in the atmosphere.

5. Vertical Wavenumber Spectra for a Single Saturated Gravity Wave: Theory

As described in section 1, there are several theoretical studies on the characteristic m spectrum with a steep slope

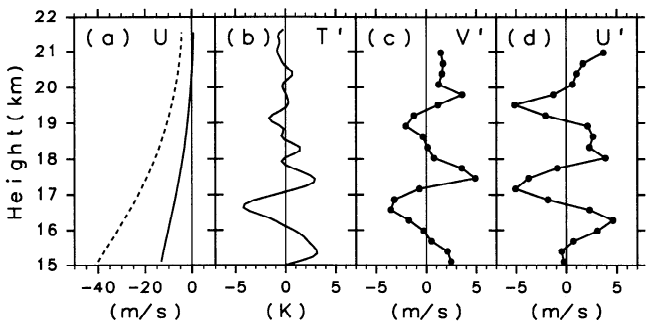

Figure 8. Vertical profiles of the (a) mean wind, (b) temperature fluctuation, (c) horizontal wind fluctuations perpendicular (90° counterclockwise) to and (d) parallel to the intrinsic phase velocity of the inertia-gravity wave. The solid and dashed curves in Figure 8a show the components parallel to and perpendicular to the intrinsic phase velocity, respectively. The dots in Figures 8c and 8d show the data positions.

of temperature and horizontal wind fluctuations, in terms of saturated gravity waves. All of the previous theoretical studies, however, ignore or do not treat explicitly this important effect of the large-scale background wind shear to the structure of gravity waves. Thus we consider the vertical wavenumber spectrum of a single saturated gravity wave propagating in a background horizontal wind having a monotonic vertical shear, using (10).

Parseval's theorem indicates that the variance, as conventionally defined, is equal to the sum of the squares of the amplitudes of each Fourier component:

$$\int P_u(m;\, t)\, dm = \frac{1}{\Delta z} \int_{z_1}^{z_2} u'^2(z;\, t)\, dz, \qquad (17)$$

where Δz denotes the height expanse from z_1 to z_2, for which the vertical wavenumber spectrum is calculated. Following *Lindzen* [1981], we assume that the integrand in the right-hand side is expressed as $[u_{\mathrm{amp}}(z) \cos \{-\omega t + \phi(z)\}]^2$, where $u_{\mathrm{amp}}(z) = |c - U(z)|$ for one saturated gravity wave with a ground-based frequency of ω. Here $\phi(z)$ is locally expressed as $m(z_0)z + \phi_0(z_0)$ around each height z_0, where $m(z_0)$ is the vertical wavenumber of the gravity wave obtained from (10) or (12). Considering the cosine factor will become 1/2 after the time averaging, we obtain

$$\int P_u(m)\, dm \sim \frac{1}{2\Delta z} \int_{z_1}^{z_2} u_{\mathrm{amp}}(z)^2\, dz, \qquad (18)$$

where $P_u(m)$ is the time average of $P_u(m;\, t)$. When the variation of U with z is monotonic, the vertical wavenumber of the saturated gravity wave also changes monotonically from $m(z_1)$ to $m(z_2)$ following (10) or (12). Hence we can change the integration variable z into m using the dispersion relation, and consequently we obtain the vertical wavenumber spectrum of horizontal wind fluctuations in a wavenumber region between $m(z_1)$ and $m(z_2)$ as

$$P_u(m) \sim \frac{u_{\mathrm{amp}}^2}{2\Delta z} \left[\left| \frac{dm}{dU} \right| \left| \frac{dU}{dz} \right| \right]^{-1} \qquad (19)$$

and almost zero elsewhere. Assuming further that the polarization relation of a monochromatic gravity wave [e.g., *Fritts*, 1984] holds true even in the process of saturation, following *Smith et al.* [1987], the spectrum of potential temperature normalized by the vertical mean $P_{\theta/\bar{\theta}}(m)$ becomes

$$P_{\theta/\bar{\theta}}(m) = \frac{N^2}{g^2} P_u(m). \qquad (20)$$

It should be noted that the results of (19) and (20) are limited in their validity to a height range in which there is no critical layer.

We obtain the m spectrum for an internal gravity wave using (10):

$$P_u(m) \sim \frac{N^3}{2m^4 \cdot \Delta z |dU/dz|}, \qquad (21)$$

$$P_{\theta/\bar{\theta}}(m) \sim \frac{N^5}{2m^4 \cdot g^2 \Delta z |dU/dz|}. \qquad (22)$$

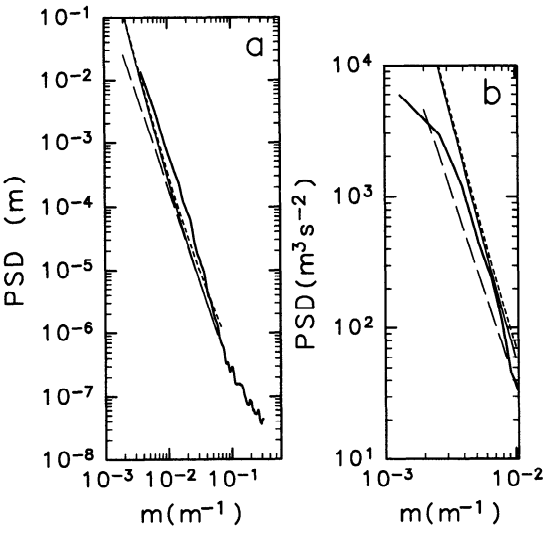

Figure 9. Vertical wavenumber spectra of the (a) normalized potential temperature and (b) horizontal wind fluctuations in the height region of 16–21 km. Dashed straight lines show the spectra by *Smith et al.* [1987], thin solid curves the theoretical spectra expressed by (18) and (19), and the dotted curves the theoretical spectra including V_z.

Equations (21) and (22) show that the vertical wavenumber spectra of horizontal wind and potential temperature fluctuations of one saturated gravity wave have a shape of m^{-4}, when vertical shear of the background wind dU/dz is constant. Using (22) for a hydrostatic inertia-gravity wave, the m spectra become

$$P_u(m) \sim \frac{N^2}{2m^3 \cdot \Delta z |dU/dz|} \sqrt{\frac{N^2}{m^2} + \frac{f^2}{k^2}}, \qquad (23)$$

$$P_{\theta/\bar{\theta}}(m) \sim \frac{N^4}{2m^3 \cdot g^2 \Delta z |dU/dz|} \sqrt{\frac{N^2}{m^2} + \frac{f^2}{k^2}}. \qquad (24)$$

These equations show that the spectral shape is m^{-4} for $m \ll |Nk/f|$, while it is m^{-3} for $m \gg |Nk/f|$. The slope of these theoretical spectra is in good agreement with previous observations.

Since the temperature and horizontal wind profiles in region A are very monochromatic, the m spectra may be explained by this theory. Although we should obtain the spectra in the region below 19 km where the Jones critical level for the inertia-gravity wave is located, the number of spectral points for such a small height region becomes small. Thus the calculation was made in an extended region of 16–21 km, including the region A. However, at least for the temperature spectra the variances above the critical level are small as found from the normalized wavelet spectra in Figure 4, and hence their modification of the spectra will not be significant. Figure 9 shows the vertical wavenumber spectra of normalized potential temperature and horizontal wind fluctuations. The meridional wind component is used for the horizontal wind spectrum, whose difference between the horizontal wind component in the direction of intrinsic phase velocity (14.5° west of north) is only 7% (about 0.3 dB). Thin solid curves indicate the theoretical spectra expressed by (23) and (24) with a dU/dz of 2.2×10^{-3} s^{-1} in the

intrinsic phase velocity direction, and the long-dashed straight lines show the saturated gravity wave spectra derived by *Smith et al.* [1987] that describe well many observational spectra, for comparison. The theoretical spectra including V_z are obtained using (15) and shown by the dotted curves which are almost overlaying the thin solid curves, i.e., the modification of m spectra by V_z is small. It is clear that the observational spectra coincide well with the theoretical spectra obtained in this study and to the same degree as with those by Smith et al. This result suggests that the vertical shear of large-scale wind structure plays an important role in determining the shape of m spectra in the middle atmosphere.

The m region in which the spectra should have the shape of (23) and (24) is estimated as follows. The lower limit of the m region in which the spectra should have the shape of (23) and (24) is estimated at about 2×10^{-3} m^{-1} from (12) by using a U of -10 m s^{-1} at the lowest height of 16 km. Note that the lower limit is almost equal to the lower limit of the m region where the height with largest variance increases with m in Figure 4. On the other hand, theoretically the m should approach infinity near the critical level but actually it does not. The upper limit of the m region having the spectral shape of (23) and (24) is evaluated by the data quality. Since the original temperature data have only one digit decimal part, and the largest peak-to-peak fluctuation amplitude is roughly equal to 15 K (about treble the standard deviation shown in Figure 2), the detectable range of power spectral amplitude is 4 orders of magnitude or more. Thus the normalized temperature spectrum of Figure 9a is believable only in the region of wavenumber with spectral amplitude larger than 10^{-6} m, namely, m smaller than about 6×10^{-2} m^{-1}. Similarly for the horizontal wind spectrum, the detectable range of power spectral amplitude can be estimated at three significant figures or more, and hence the whole range displayed in Figure 9b is believable. The thin solid curves in Figure 9 are drawn only in the m region where the spectra should accord with the theory of (23) and (24).

6. Discussion

The theoretical m spectra were derived under the very idealized condition that a single saturated gravity wave propagates vertically, and the condition is not always valid. According to the statistical study by S94, the horizontal propagation direction of inertia-gravity waves depends on height, showing that the fluctuation field consists of multiple waves. It should be noted here that the vertical mean spectrum used for normalization of the wavelet spectra in Figure 4 has a steep slope at larger m values. This vertical mean spectrum is probably due to the superposition of multiple gravity waves whose amplitudes are much weaker than the dominant inertia-gravity wave examined in detail. However, it is likely that the superposed waves are, respectively, affected by the vertical shear of large-scale background wind and will form the steeply sloped m spectra.

It is important that the inertia-gravity wave examined in this study has almost zero ground-based phase speed. Typical gravity waves having such a ground-based phase speed are topographically forced waves. The wind near the surface blew almost southward with a magnitude larger than 10 m s^{-1} when the very clear wave structure in Figure 5 was observed (not shown). The direction of intrinsic phase velocity of gravity waves excited in the southward wind must be biased toward northward, which is consistent with the estimation using the hodograph of horizontal wind fluctuations and from the phase difference between temperature and horizontal wind fluctuations. Thus the inertia-gravity wave examined here is likely to have been excited by the topographical effect near the ground.

If this interpretation is the case, the gravity wave should be present also in the troposphere. However, in Figure 5 we can recognize only a few inversion layers rather than sinusoidal wavelike structure in the troposphere. *Hines* [1989] made a case study of a tropopausal wave observed at Arecibo and also interpreted it as a mountain wave. He attributed no wave structure in the troposphere to small N and large U which modulate the vertical wavelength to be longer (see (10)). Mountain waves observed by the MU radar in the troposphere were described by *Sato* [1990] using vertical wind data. Although quasi-stationary mountain waves are hardly distinguished from the background wind field only using the horizontal wind data at one location, we can examine mountain waves using vertical wind data since the large-scale background vertical wind field is very weak. Sato showed that the vertical wavelength of mountain waves observed as vertical wind disturbances in the troposphere are very long and the phase lines are almost vertical. Similar vertical wind disturbances having long vertical wavelengths are seen in the case of this study (not shown). This fact is consistent with the interpretation of mountain waves.

It is known that topographically forced gravity waves have large energy in the lower stratosphere [*Fritts and Nastrom*, 1992; S94]. The large-scale background wind is strong due to the subtropical westerly jet around the tropopause and very weak near the height of 20 km in all seasons. Modification of the gravity wave structure by the large-scale background wind shear, similar to the case examined in this study, possibly occurs.

S94 also showed that a systematic tendency of the increase of m with altitude in the lower stratosphere is observed in all seasons. This fact indicates that the gravity wave field is controlled not simply by the stability described with the Brunt-Väisälä frequency but also by other background field structures. The vertical wind shears below and above the global-scale jet around the tropopause and in the mesosphere are one of the most likely candidates.

7. Summary and Concluding Remarks

We examined the vertical variation of vertical wavenumber spectra of temperature fluctuations using the recently developed wavelet method. Analysis was made of observational data from October 1988. It was clear that the variance distribution in m space was not uniform even in the stratosphere and that the height position having large variance depended on m. By analyzing the phase structure of the temperature and horizontal wind fluctuations under the assumption that these fluctuations were due to one inertia-gravity wave, we obtained the ground-based horizontal phase velocity without any inconsistency. Using the phase velocity, we estimated the vertical variation of the vertical wavelength due to the large-scale background wind having a vertical shear. The result explained well the observed fluctuations and was consistent with the wavelet spectra. We also considered theoretically the m spectra for a single

gravity wave, including the modification of m by the large-scale background wind having a vertical shear, and the saturation of amplitudes due to local convective instability. Both the amplitude and the slope of the theoretical spectra were almost in accord with the observations.

Our theory in the present paper has been developed under the assumption that the wave field is dominated by a quasi-monochromatic wave. It is clearly necessary to extend the spectral theory to the general case where the wind and temperature fields are a superposition of multiple gravity waves, as is usually observed. The wavelet method we employed in the present paper provides us with a simultaneous decomposition by position and scale and is found to be powerful even for the case of superposed gravity waves. Further analysis is expected for the observed fluctuations in the middle atmosphere.

Acknowledgments. The present authors thank Jun-Ichi Yano for his valuable discussions on the derivation of the equation (21). Thanks are also extended to Charles Kilburn for his kindly checking English of the original manuscript and to two anonymous reviewers for their critical reading and comments. The MU radar belongs to and is operated by the Radio Atmospheric Science Center of Kyoto University. This paper was presented at the International Symposium on Middle Atmosphere Science, Kyoto, March 1992.

References

Daubechies, I., Orthonormal bases of compactly supported wavelets, *Commun. Pure Appl. Math., XLI*, 909–996, 1988. Daubechies, I., *Ten Lectures on Wavelets*, 357 pp., Society for Industrial and Applied Mathematics, Philadelphia, Penn., 1992.

Dewan, E. M., and R. E. Good, Saturation and the "universal" spectrum for vertical profiles of horizontal scalar winds in the atmosphere, *J. Geophys. Res., 91*, 2742–2748, 1986.

Fritts, D. C., Gravity wave saturation in the middle atmosphere: A review of theory and observations, *Rev. Geophys., 22*, 275–308, 1984.

Fritts, D. C., and G. D. Nastrom, Sources of mesoscale variability of gravity waves, II, Frontal, convective, and jet stream excitation, *J. Atmos. Sci., 49*, 110–127, 1992.

Fukao, S., T. Sato, T. Tsuda, S. Kato, K. Wakasugi, and T. Makihira, The MU radar with an active phased array system, 1, Antenna and power amplifiers, *Radio Sci., 20*, 1155–1168, 1985a.

Fukao, S., T. Tsuda, T. Sato, S. Kato, K. Wakasugi, and T. Makihira, The MU radar with an active phased array system, 2, In-house equipment, *Radio Sci., 20*, 1169–1176, 1985b.

Gardner, C. S., and D. G. Voelz, Lidar studies of the nighttime sodium layer over Urbana, Illinois, 2, Gravity waves, *J. Geophys. Res., 92*, 4673–4694, 1987.

Hines, C. O., Tropopausal mountain waves over Arecibo: A case study, *J. Atmos. Sci., 46*, 476–488, 1989.

Hines, C. O., The saturation of gravity waves in the middle atmosphere, I, Critique of linear-instability theory, *J. Atmos. Sci., 48*, 1348–1359, 1991a.

Hines, C. O., The saturation of gravity waves in the middle atmosphere, II, Development of Doppler-spread theory, *J. Atmos. Sci., 48*, 1360–1379, 1991b.

Jones, W. L., Propagation of internal gravity waves in the fluids with shear and rotation, *J. Fluid Mech., 30*, 439–448, 1967.

Lindzen, R. S., Turbulence and stress due to gravity wave and tidal breakdown, *J. Geophys. Res., 86*, 9707–9714, 1981.

Meyer, Y., Principe d'incertitude, bases hilbertiennes et algebres d'operateurs (in French), paper presented at Seminaire Bourbaki, 1985–1986, 1985.

Sato, K., Vertical wind disturbances in the troposphere and lower stratosphere observed by the MU radar, *J. Atmos. Sci., 47*, 2803–2817, 1990.

Sato, K., A statistical study on structure, saturation and sources of inertio-gravity waves in the lower stratosphere observed with the MU radar, *J. Atmos. Terr. Phys., 56*, 755–774, 1994.

Smith, S. A., D. C. Fritts, and T. E. VanZandt, Evidence of a saturation spectrum of atmospheric gravity waves, *J. Atmos. Sci., 44*, 1404–1410, 1987.

Stromberg, J. O., *A Modified Franklin System and Higher Order Spline Systems on R^n as Unconditional Bases for Hardy Spaces, Wadsworth Math. Ser.*, vol. 2, edited by W. Becker et al., pp. 475–493, 1982.

Tsuda, T., T. Inoue, D. C. Fritts, T. E. VanZandt, S. Kato, T. Sato, and S. Fukao, MST radar observations of a saturated gravity wave spectrum, *J. Atmos. Sci., 46*, 2440–2447, 1989.

VanZandt, T. E., A model for gravity wave spectra observed by Doppler sounding systems, *Radio Sci., 20*, 1323–1330, 1985.

Weinstock, J., Saturated and unsaturated spectra of gravity waves, and scale dependent diffusion, *J. Atmos. Sci., 47*, 2211–2225, 1990.

Wilson, R., M. L. Chanin, and A. Hauchecorne, Gravity waves in the middle atmosphere observed by Rayleigh lidar, 2, *Climatology, J. Geophys. Res., 96*, 5169–5183, 1991.

Yamada, M., and K. Ohkitani, Orthonormal wavelet expansion and its application to turbulence, *Prog. Theor. Phys., 83*, 819–823, 1990.

Yamada, M., and K. Ohkitani, An identification of energy cascade in turbulence by orthonormal wavelet analysis, *Prog. Theor. Phys., 86*, 799–815, 1991a.

Yamada, M., and K. Ohkitani, Orthonormal wavelet analysis of turbulence, *Fluid Dyn. Res., 8*, 101–115, 1991b.

K. Sato, Center for Climate Research, University of Tokyo, 4-6-1 Komaba, Meguro-ku, Tokyo 153, Japan.

M. Yamada, Department of Mathematical Sciences, University of Tokyo, Tokyo 153, Japan.

(Received October 15, 1993; revised June 22, 1994; accepted July 11, 1994.)